Numerical solution of the time-dependent Schrödinger equation for H_2^+ ion with application to high-harmonic generation and above-threshold ionization

B. Fetić[1] and D. B. Milošević[1,2,3]

[1]*Faculty of Science, University of Sarajevo, Zmaja od Bosne 35, 71000 Sarajevo, Bosnia and Herzegovina*

[2]*Academy of Sciences and Arts of Bosnia and Herzegovina, Bistrik 7, 71000 Sarajevo, Bosnia and Herzegovina*

[3]*Max-Born-Institut, Max-Born-Straße 2a, D-12489 Berlin, Germany*

(Received 12 January 2017; published 31 May 2017)

Time evolution of the bound state of a molecular hydrogen cation in an intense, linearly polarized laser field is investigated by solving the full three-dimensional time-dependent Schrödinger equation. Our method is based on the Born-Oppenheimer and dipole approximations, and the wave function is expanded in finite series using B-spline functions and spherical harmonics in prolate spheroidal coordinates. After solving the stationary Schrödinger equation, the initial state is propagated under the influence of the laser field employing the Crank-Nicolson propagator. Using this method we calculate and present high-harmonic photon spectra and above-threshold ionization angle-resolved electron spectra.

DOI: 10.1103/PhysRevE.95.053309

I. INTRODUCTION

The interaction between intense laser fields and atomic and molecular systems is a subject of great current interest, both from experimental and theoretical points of view. This interaction leads to highly nonlinear strong-field phenomena, and much of our knowledge about such processes comes from the study of high-order harmonic generation (HHG) and above-threshold ionization (ATI) (see, for example, the review articles [1–3] and references therein). To describe such processes it is necessary to numerically solve the many-electron time-dependent Schrödinger equation (TDSE) which is beyond the capability of current computers. Because of this bottleneck, the TDSE is usually solved in the single-active electron (SAE) approximation in which only the valence electron interacts with the laser pulse, while the core electrons are frozen. This approximation has already been used for atomic systems to describe HHG and ATI (see, for example, the review articles [4–6] and implementations [7,8]). Typical time consumption of the numerical algorithm for a fully three-dimensional TDSE within the SAE approximation on a single desktop PC ranges from a few minutes to a few days, depending on the laser pulse duration, wavelength, intensity, and nature of the problem.

Molecular systems introduce more complexity into the TDSE [1]. That is why other theoretical models—such as molecular Ammosov-Delone-Krainov theory [9] and molecular strong-field approximation (MSFA) theory [10,11]—are often used to study the ionization of molecular systems. For example, for more intense laser fields the improved MSFA is applied to HHG [12] and high-order ATI of diatomic [13] and polyatomic [14] molecules. It is necessary to test the above-mentioned models by solving the TDSE for molecular systems. This is possible for the simplest and smallest molecule, the H_2^+ ion. This molecule is relevant per se (for example, in environments ranging from interstellar chemistry to fusion reactors) but, in the context of strong field physics, it is more important since the symmetry properties of most diatomic molecular orbitals can be reproduced by choosing appropriate H_2^+ orbitals.

The TDSE for H_2^+ has been solved using various methods and in various contexts (as an incomplete list we mention [15–19] and references therein). However, for laser fields having long wavelengths ($\gtrsim$800 nm) and high intensities ($>10^{14}$ W/cm^2) there is a limited number of *ab initio* full three-dimensional calculations of HHG and ATI spectra of H_2^+. New and more efficient methods of calculations are desirable.

In this paper we describe a numerical method for solving the TDSE of a one-electron hydrogen molecular cation using B-spline functions and spherical harmonics to represent the wave function in the prolate spheroidal coordinates. This paper is organized as follows. In Sec. II we introduce numerical method for solving the stationary Schrödinger equation. The initial state obtained by this method is propagated in time using an algorithm described in Sec. III. In the last two sections, application to HHG and ATI is presented. Atomic units (a.u.; $\hbar = 1, 4\pi\varepsilon_0 = 1, |e| = 1,$ and $m_e = 1$) are used throughout the paper, unless stated otherwise.

II. MOLECULAR HAMILTONIAN IN PROLATE SPHEROIDAL COORDINATES

A one-electron diatomic molecule in the Born-Oppenheimer and fixed-nuclei approximation is described by the Hamiltonian

$$H_0 = -\frac{1}{2}\nabla^2 - \frac{Z_1}{r_1} - \frac{Z_2}{r_2} + \frac{Z_1 Z_2}{R}, \tag{1}$$

where Z_1 and Z_2 are nuclear charges and r_1 and r_2 are electron distances from nuclei. The last term in (1) is the Coulomb interaction of the two nuclei, which is constant and can be omitted. We assume that the internuclear axis is aligned along the z axis so that $\mathbf{R} = R\mathbf{e}_z$. Electron distances from nuclei are evaluated as $r_1 = |\mathbf{r} + \frac{R}{2}\mathbf{e}_z|$ and $r_2 = |\mathbf{r} - \frac{R}{2}\mathbf{e}_z|$. For the diatomic molecule there are special coordinates which take care of the Coulomb singularities at the two nuclei, namely the prolate spheroidal coordinates (ξ, η, φ), where φ is the angle around the z axis and

$$\xi = \frac{r_1 + r_2}{R}, \quad \xi \in [1, \infty), \tag{2}$$

$$\eta = \frac{r_1 - r_2}{R}, \quad \eta \in [-1, 1]. \tag{3}$$

These coordinates have been successfully used in Hartree-Fock calculations for diatomic molecules [20–22]. The connection between the Cartesian coordinates and the prolate spheroidal coordinates is given by

$$x = \frac{R}{2}\sqrt{(\xi^2-1)(1-\eta^2)}\cos\varphi, \tag{4}$$

$$y = \frac{R}{2}\sqrt{(\xi^2-1)(1-\eta^2)}\sin\varphi, \tag{5}$$

$$z = \frac{R}{2}\xi\eta, \tag{6}$$

with the volume element defined as $d\tau = \frac{R^3}{8}(\xi^2-\eta^2)d\xi\, d\eta\, d\varphi$.

Hamiltonian (1) in prolate spheroidal coordinates is

$$H_0 = -\frac{2}{R^2(\xi^2-\eta^2)}\left[\frac{\partial}{\partial\xi}(\xi^2-1)\frac{\partial}{\partial\xi} + \frac{\partial}{\partial\eta}(1-\eta^2)\frac{\partial}{\partial\eta} + \left(\frac{1}{\xi^2-1}+\frac{1}{1-\eta^2}\right)\frac{\partial^2}{\partial\varphi^2}\right] + V(\xi,\eta), \tag{7}$$

where $V(\xi,\eta)$ is the Coulomb interaction:

$$V(\xi,\eta) = -2\frac{(Z_1+Z_2)\xi-(Z_1-Z_2)\eta}{R(\xi^2-\eta^2)}. \tag{8}$$

We will limit our study to a homonuclear H_2^+ molecular ion with $Z_1 = Z_2 = 1$, since this molecule has only one active electron and is a good starting point to test the validity of our numerical method. It can be shown that the Hamiltonian (7) commutes with the projection operator L_z of the electron angular momentum along the z axis, meaning that L_z is a constant of motion. Thus, the wave function in prolate spheroidal coordinates can be written as [23]

$$\Psi(\xi,\eta,\varphi) = \psi(\xi,\eta)\frac{\exp(im\varphi)}{\sqrt{2\pi}}. \tag{9}$$

When this function is introduced into the Schrödinger equation, the factor $\exp(im\varphi)$ cancels and the quantum number m appears in this equation as m^2 so that the number $\lambda = |m|(m = 0, \pm 1, \pm 2, \dots)$ is used to describe one-electron orbitals. For homonuclear molecules, Hamiltonian (7) also possesses inversion symmetry with respect to the midpoint between nuclei due to the Coulomb potential property $V(\xi,\eta) = V(\xi,-\eta)$. This means that the wave functions $\psi(\xi,\eta)$ are even (*gerade*) or odd (*ungerade*) functions.

We will solve the Schrödinger equation $H_0\Psi(\xi,\eta,\varphi) = E\Psi(\xi,\eta,\varphi)$ by expressing wave functions in terms of B-spline functions and spherical harmonics:

$$\Psi(\xi,\Omega,t) \approx \sum_{i=1}^{N_\xi-1}\sum_{l=|m|}^{L} a_{il}(t)B_i(\xi)(\xi^2-1)^{|m|/2}Y_l^m(\Omega), \tag{10}$$

where $\eta = \cos\theta$ and N_ξ is the number of B-spline functions used. For a review of the B-spline functions see [24]. Expansion coefficients a_{il} are time dependent when we propagate the wave function under the influence of the laser field. The sum over spherical harmonics is truncated at L and the interval of the ξ coordinate is limited to $[1,\xi_{\max}]$. Factor $(\xi^2-1)^{|m|/2}$ is used in the B-spline expansion in order to avoid singularities at $\xi = 1$. The wave function should also satisfy the boundary condition $\Psi(\xi_{\max},\eta,\varphi) = 0$. This condition is fulfilled by excluding the last B-spline function B_{N_ξ} from the expansion (10). The symmetry of the wave functions is included in the spherical harmonics since they also possess inversion symmetry:

$$Y_l^m(\pi-\theta,\varphi+\pi) = (-1)^l Y_l^m(\theta,\varphi). \tag{11}$$

For *gerade* states we use only even l in expansion (10) and for *ungerade* states we use only odd l. For example, for the σ_g state ($\lambda = 0$) $l = 0,2,4,\dots,L$; for the σ_u state $l = 1,3,5,\dots,L$; for the π_g state ($\lambda = 1$) $l = 2,4,6,\dots,L$; for the π_u state $l = 1,3,5,\dots,L$, etc. Using this property of the spherical harmonics, there is no need to define different basis sets for even and odd m as done in the method of finite-element discrete-variable representation [25,26].

The next step is to transform the Schrödinger equation into a standard generalized eigenvalue problem. This is accomplished by inserting wave function (10) into the Schrödinger equation and multiplying by $(\xi^2-1)^{|m|/2}B_j(\xi)Y_k^{m*}(\theta,\varphi)$ and finally integrating over $d\tau$. In this way we obtain matrix elements of the molecular Hamiltonian:

$$(H_0)_{ij}^{kl} = -\delta_{k,l}\frac{R}{4}\int_1^{\xi_{\max}} B_i(\xi^2-1)^{|m|/2}\left[\frac{\partial}{\partial\xi}(\xi^2-1)\frac{\partial}{\partial\xi} - \frac{m^2}{\xi^2-1} + 2R\xi\right]B_j(\xi^2-1)^{|m|/2}d\xi + \delta_{k,l}l(l+1)\frac{R}{4}\int_1^{\xi_{\max}} B_iB_j(\xi^2-1)^{|m|}d\xi. \tag{12}$$

The last term was evaluated using the generalized Legendre differential equation [27]:

$$\left[\frac{\partial}{\partial\eta}(1-\eta^2)\frac{\partial}{\partial\eta} + l(l+1) - \frac{m^2}{1-\eta^2}\right]P_l^m(\eta) = 0. \tag{13}$$

The right-hand side of the Schrödinger equation leads to the overlap matrix element:

$$(S)_{ij}^{kl} = \delta_{k,l}\frac{R^3}{8}\int_1^{\xi_{\max}} B_iB_j\xi^2(\xi^2-1)^{|m|}d\xi - \frac{R^3}{8}\int_1^{\xi_{\max}} B_iB_j(\xi^2-1)^{|m|}d\xi\left\{c_{l-1}^m c_{l-2}^m\delta_{k,l-2} + \left[\left(c_{l-1}^m\right)^2 + \left(c_l^m\right)^2\right]\delta_{k,l} + c_l^m c_{l+1}^m\delta_{k,l+2}\right\}, \tag{14}$$

where we have used the identity

$$\cos\theta\, Y_l^m(\theta,\varphi) = c_{l-1}^m Y_{l-1}^m(\theta,\varphi) + c_l^m Y_{l+1}^m(\theta,\varphi), \tag{15}$$

$$c_l^m = \sqrt{\frac{(l+1)^2-m^2}{(2l+1)(2l+3)}}. \tag{16}$$

Integrals over η are evaluated in closed analytical form, which is another advantage of the basis set expansion we used. Since B-spline functions are piecewise polynomial functions, integrals involving B-spline functions are calculated using the Gauss-Legendre formula [28]. The Hamiltonian matrix $\mathbf{H}_0$ is diagonal in l-space but the overlap matrix $\mathbf{S}$ is not. Furthermore, these matrices are banded which further reduces computation time. Eigenvalues and eigenvectors of the generalized eigenvalue problem $\mathbf{H_0}\cdot\mathbf{a} = E\mathbf{S}\cdot\mathbf{a}$ are determined

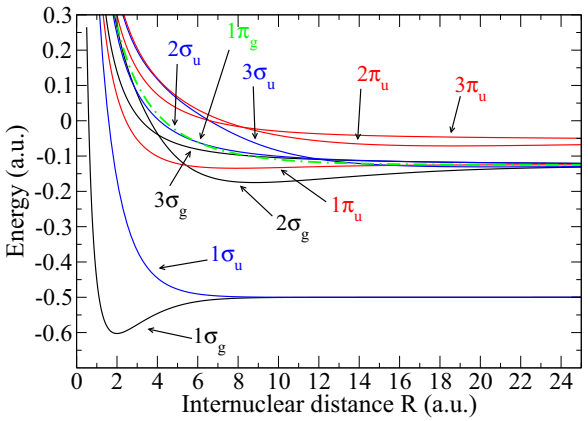

FIG. 1. Potential curves for several lowest-lying bound states.

using LAPACK subroutine DSPGVX [29]. In Fig. 1 we show potential curves for σ and π states as functions of the internuclear distance.

Calculated eigenvalues for several lowest lying states for internuclear distance $R = 2$ a.u. are given in Table I with omitted nuclear potential energy. We compared these calculated eigenvalues with already published results [16,30] and found a good agreement. Eigenvalues were calculated using up to 20 spherical harmonics and 80 B-spline functions of order 10 with $\xi_{\max} = 60$. By solving the stationary Schrödinger equation we were able to test the accuracy of the basis set expansion (10) and to obtain an initial state for the TDSE.

III. TIME EVOLUTION OF THE INITIAL STATE

A one-electron molecule exposed to an intense laser field is described by the TDSE:

$$i\frac{\partial \Psi}{\partial t} = H\Psi, \quad H = H_0 + V_I(t), \tag{17}$$

where operator $V_I(t)$ represents the electron-laser interaction in the dipole approximation. In the length gauge this interaction is given by $V_L(t) = \mathbf{r}\cdot\mathbf{E}(t)$, and in velocity gauge by $V_V(t) = -i\mathbf{A}(t)\cdot\hat{\mathbf{p}}$, where $\mathbf{A}(t) = -\int^t \mathbf{E}(t')dt'$ is the vector potential of the laser field.

Under the influence of the laser field, the parity of the wave function breaks down and in the expansion (10) we have to include both even and odd spherical harmonics. For a linearly polarized laser field along the internuclear axis, axial symmetry is preserved but the same conclusion is not valid for an arbitrarily polarized laser field. We assume that the laser electric field is linearly polarized along the internuclear axis. The interaction operator in velocity gauge is given by

$$\begin{aligned} V_V(t) &= -iA(t)\frac{\partial}{\partial z} \\ &= -iA(t)\frac{2}{R}\frac{1}{\xi^2-\eta^2}\left[(\xi^2-1)\eta\frac{\partial}{\partial\xi} + (1-\eta^2)\xi\frac{\partial}{\partial\eta}\right], \end{aligned} \tag{18}$$

while in length gauge it is

$$V_L(t) = \frac{R}{2}\xi\eta E(t). \tag{19}$$

Matrix elements corresponding to the interaction operator in velocity gauge are given by

$$\begin{aligned} (V_V)_{ij}^{kl} = &-i\frac{R^2A(t)}{4}\int_1^{\xi_{\max}} B_i\frac{dB_j}{d\xi}(\xi^2-1)^{|m|+1}d\xi \\ &\times\left[c_{l-1}^m\delta_{k,l-1} + c_l^m\delta_{k,l+1}\right] \\ &-i\frac{R^2A(t)}{4}|m|\int_1^{\xi_{\max}} B_iB_j(\xi^2-1)^{|m|}\xi d\xi \\ &\times\left[c_{l-1}^m\delta_{k,l-1} + c_l^m\delta_{k,l+1}\right] \\ &-i\frac{R^2A(t)}{4}\int_1^{\xi_{\max}} B_iB_j(\xi^2-1)^{|m|}\xi d\xi \\ &\times\left[(l+1)c_{l-1}^m\delta_{k,l-1} - lc_l^m\delta_{k,l+1}\right]. \end{aligned} \tag{20}$$

The last term was evaluated using the identity

$$(1-\eta^2)\frac{\partial}{\partial\eta}Y_l^m = (l+1)c_{l-1}^mY_{l-1}^m - lc_l^mY_{l+1}^m. \tag{21}$$

As we can notice, the matrix $\mathbf{V}_V$ is a narrow-banded matrix coupling the $l-1$ and $l+1$ blocks. Matrix elements corresponding to the interaction operator in length gauge are given by

$$\begin{aligned} (V_L)_{ij}^{kl} = &\frac{R^4}{16}E(t)\int_1^{\xi_{\max}}(\xi^2-1)^{|m|}\xi^3B_iB_jd\xi \\ &\times\left[c_{l-1}^m\delta_{k,l-1} + c_l^m\delta_{k,l+1}\right] \\ &-\frac{R^4}{16}E(t)\int_1^{\xi_{\max}}(\xi^2-1)^{|m|}\xi B_iB_jd\xi \\ &\times\left\{c_{l-1}^mc_{l-2}^mc_{l-3}^m\delta_{k,l-3} + \left[c_{l-1}^m\left(c_{l-2}^m\right)^2 + \left(c_{l-1}^m\right)^3\right.\right. \\ &+c_{l-1}^m\left(c_l^m\right)^2\left]\delta_{k,l-1} + \left[c_l^m\left(c_{l-1}^m\right)^2 + \left(c_l^m\right)^3\right.\right. \\ &\left.\left.+c_l^m\left(c_{l+1}^m\right)^2\right]\delta_{k,l+1} + c_l^mc_{l+1}^mc_{l+2}^m\delta_{k,l+3}\right\}, \end{aligned} \tag{22}$$

TABLE I. Bound state energies of the molecular hydrogen ion for internuclear distance $R = 2$ a.u. with omitted nuclear potential energy $1/R$.

State	Eigenvalues (a.u.)	Eigenvalues from [30]	Eigenvalues from [16]
$1\sigma_g$	−1.102 634 214 494 909 7	−1.102 634 214 494 946 4	−1.102 634 214 5
$1\sigma_u$	−0.667 534 392 202 603 5	−0.667 534 392 202 382 9	−0.667 534 392 20
$1\pi_u$	−0.428 771 819 896 048 5	−0.428 771 819 895 856 4	−0.428 771 819 90
$2\sigma_g$	−0.360 864 875 339 372 1	−0.360 864 875 339 503 8	−0.360 864 875 34
$2\sigma_u$	−0.255 413 165 086 447 2	−0.255 413 165 086 484 5	−0.255 413 165 09
$1\pi_g$	−0.226 699 626 643 484 7	−0.226 699 626 643 657 6	−0.226 699 626 64
$1\delta_g$	−0.212 732 681 811 212 5	−0.212 732 681 810 763 1	−0.212 732 681 81

so that the interaction matrix also couples $l-3$ and $l+3$ blocks, which in turn gives more nonzero off-diagonal elements than the interaction matrix in velocity gauge.

The TDSE is solved by approximating the time-evolution operator with the Crank-Nicolson approximation [7,31]:

$$\mathbf{a}(t+\Delta t) = \frac{\mathbf{S}-\frac{i\Delta t}{4}\mathbf{V}_I(t+\Delta t)}{\mathbf{S}+\frac{i\Delta t}{4}\mathbf{V}_I(t+\Delta t)} \times \frac{\mathbf{S}-\frac{i\Delta t}{2}\mathbf{H_0}}{\mathbf{S}+\frac{i\Delta t}{2}\mathbf{H_0}} \times \frac{\mathbf{S}-\frac{i\Delta t}{4}\mathbf{V}_I(t)}{\mathbf{S}+\frac{i\Delta t}{4}\mathbf{V}_I(t)}\mathbf{a}(t), \tag{23}$$

where the elements of the overlap matrix S are defined by Eq. (14). This propagator preserves the norm of the wave function. There are other forms of the Crank-Nicolson propagator (see for example [17,26,32]) defined by rearranging terms in (23). We find that these forms of the Crank-Nicolson propagator cannot give desirable numerical accuracy. This conclusion has also been emphasized in [31].

If a part of the wave function reaches the boundary at $\xi = \xi_{\max}$, it will be reflected back, causing unphysical interference with the initial wave. This effect can be overcome by using an absorber in the form of a negative imaginary potential in the region close to the boundary wall [33]. In our HHG spectrum calculations we use a negative imaginary potential in the form of

$$V_{\text{abs}}(\xi) = \begin{cases} -iW_0(\xi-\xi_0)^\kappa & \text{for } \xi_0 \leqslant \xi \leqslant \xi_{\max}, \\ 0 & \text{otherwise}, \end{cases} \tag{24}$$

where $10^{-3} \leqslant W_0 \leqslant 10^{-2}$, $\xi_{\max} - \xi_0 \geqslant 40$ with $\kappa = 1$ or 2.

All matrices in the time evolution algorithm are banded and these systems of linear equations can be solved using the appropriate LAPACK subroutine together with the use of the optimized BLAS library [34,35].

IV. APPLICATION TO HIGH-ORDER HARMONIC GENERATION

In this section we present an application of the developed propagation algorithm to high-order harmonic generation. HHG is a highly nonlinear strong-field phenomenon which can be explained by the three-step recollision model [5,36]: (a) the electron under the influence of the laser field is "born" in the continuum, (b) then it is accelerated by the applied laser field and eventually is driven back to the parent ion, and (c) during recombination of the electron with the parent ion a high-order harmonic is emitted. This three-step model predicts that the maximum harmonic order N_m is determined by the relation

$$N_m\omega = 1.325I_p + 3.173U_p, \tag{25}$$

where I_p is the ionization potential of the target and U_p is the ponderomotive energy of the electron, given in atomic units as $U_p = I/(4\omega^2)$, where I and ω are the laser field intensity and frequency, respectively. The factor 1.325 in above equation is a semiclassical correction [37,38].

The intensity of the emitted harmonic of frequency Ω is proportional to the Fourier transform of the time-dependent dipole acceleration [39]:

$$I(\Omega) = \left| \frac{1}{t_f - t_i} \int_{t_i}^{t_f} d_A(t) \exp(-i\Omega t) dt \right|^2. \tag{26}$$

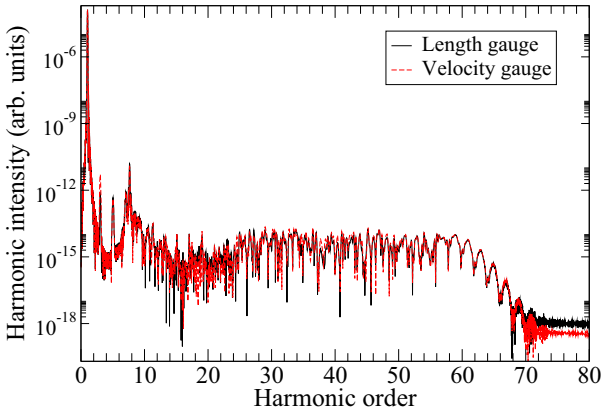

FIG. 2. Comparison of the HHG spectra calculated using length and velocity gauges for a laser pulse of intensity $I = 3 \times 10^{14}$ W/cm^2, wavelength $\lambda = 800$ nm, and duration of 18 optical cycles. Initial state is $1\sigma_g$. For other parameters see the text.

The dipole acceleration

$$d_A(t) = -\langle\Psi(t)|\frac{\partial V}{\partial z}|\Psi(t)\rangle - E(t) \tag{27}$$

is calculated using the Gauss-Legendre integration method for double integrals over the variables ξ and η [28].

The HHG spectrum is calculated using length or velocity gauge for the laser-molecule interaction, with the electric field given by

$$E(t) = E_0 \cos^2\left(\frac{\pi t}{\tau}\right)\cos(\omega t + \phi), \quad t \in \left[-\frac{\tau}{2}, \frac{\tau}{2}\right], \tag{28}$$

with the carrier-envelope phase ϕ set to zero. All results presented in this and the following section are obtained for the equilibrium internuclear distance $R = 2$ a.u.

With initial state $1\sigma_g$, laser field intensity $I = 3 \times 10^{14}$ W/cm^2, and a pulse duration of 18 optical cycles, we find that it is sufficient to use up to 36 spherical harmonics in order to achieve the convergence in length gauge. In velocity gauge the convergence is achieved with 20 spherical harmonics for the same laser field parameters. This is not surprising, since it is known that the TDSE results converge faster in velocity gauge [40]. In general, we use velocity gauge. In Fig. 2 we compare HHG spectra obtained in length and velocity gauges and, as we can notice, the HHG spectrum is gauge invariant as it should be. Both spectra are calculated using $N_\xi = 200$ B-splines of order $k = 10$, with $\xi_{\max} = 180$, $\xi_0 = 90$, and $\Delta t = 0.05$ a.u. For harmonic orders above 71st, which are far beyond the cutoff, the harmonic intensity is of the order 10^{-18} arb. units and, due to numerical error by finite precision of computation, the velocity and length gauge results are different.

Semiclassical formula (25) predicts that the cutoff of the HHG spectrum is at the 61st harmonic, which is in excellent agreement with our TDSE calculations.

In Fig. 3 we show HHG spectra calculated using velocity gauge for different laser field intensities and wavelength $\lambda = 800$ nm for the $1\sigma_u$ initial state. Other laser field parameters are the same as in previous calculations. Cutoff positions are at the 39th, 51st, and 63rd harmonics for given

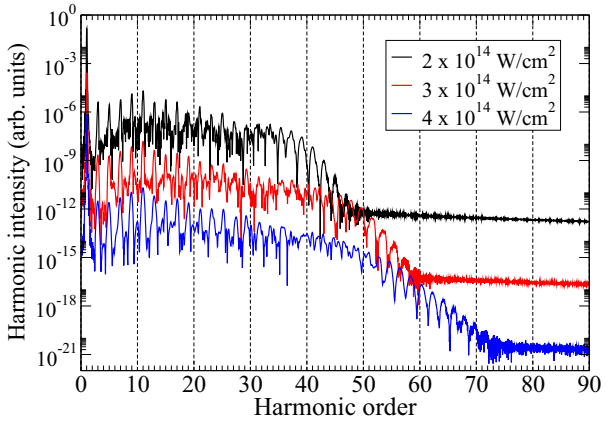

FIG. 3. HHG spectra calculated using velocity gauge for different laser field intensities and wavelength $\lambda = 800$ nm. Initial state is $1\sigma_u$. Spectra are shifted vertically for clarity. Other laser parameters are the same as in Fig. 2.

intensities. Notice that the results of Figs. 2 and 3, for the same laser parameters, looks differently due to different initial states ($1\sigma_g$ having ionization potential 30.00 eV vs $1\sigma_u$ having $I_p = 18.16$ eV).

V. APPLICATION TO ABOVE-THRESHOLD IONIZATION

We now focus our attention to the above-threshold ionization of the H_2^+ molecular ion. In this process an atom absorbs more photons than the minimum number required for ionization [2,41]. The overall characteristics of the ATI spectra are peaks separated by the photon energy and shifted by the ponderomotive energy. Because of energy conservation, the energy corresponding to an ATI peak originating from ionization with absorption of n photons is $E = n\omega - (I_p + U_p)$.

From a numerical point of view, calculations of the photoelectron ionization probability are more time consuming than calculations of the HHG spectrum for the same laser field parameters. In order to include photoelectrons with large kinetic energy, a very large grid is required.

The TDSE solver provides the wave function at the end of propagation $\Psi(t_f)$ and this wave function contains all the information about physical observables. The photoelectron spectrum can be extracted through the projection of the final wave function to the continuum states satisfying the appropriate incoming boundary condition. Since the field-free Hamiltonian (7) is completely separable in the prolate spheroidal coordinates, continuum states are built from the "angular" $\Xi_{|m|}(\eta)$ and "radial" $\Pi_{|m|}(\xi)$ parts of the wave function satisfying equations

$$\left[\frac{d}{d\eta}(1-\eta^2)\frac{d}{d\eta} - \frac{m^2}{1-\eta^2} - c^2\eta^2 + A\right]\Xi_{|m|}(\eta) = 0, \quad (29)$$

$$\left[\frac{d}{d\xi}(\xi^2-1)\frac{d}{d\xi} - \frac{m^2}{1-\eta^2} + c^2\xi^2 + 2R\xi - A\right]\Pi_{|m|}(\xi) = 0, \quad (30)$$

with $c = kR/2 (k = \sqrt{2E})$, and A being the separation constant. The angular equation is solved by expanding $\Xi_{|m|}(\eta)$ into a series of normalized associated Legendre polynomials [42]:

$$\Xi_{|m|}(\eta) = \sum_{r=0} d_r(c) V_{r+|m|}^{|m|}(\eta),$$

where $V_{r+|m|}^{|m|}(\eta) = M_{r+|m|}^{|m|} P_{r+|m|}^{|m|}(\eta)$ are normalized associated Legendre polynomials, with $M_{r+|m|}^{|m|}$ being normalization constants. This method converts the angular equation into an eigenvalue problem which can be solved by the LAPACK subroutine DSBEVD. The separation constants are labeled by $A_{|m|q}$, where q ($q = 0,1,2,\ldots$) represents the number of nodes of the function $\Xi_{|m|q}(\eta)$ in the interval $\eta \in [-1,1]$. After obtaining eigenvalues $A_{|m|q}$, the radial equation is numerically solved by the finite-difference scheme proposed by Killingbeck [43] and described in detail in [44]. The phase shifts are obtained by matching the numerical solution of the radial equation with the asymptotic solution when $\xi = \xi_{max} \gg 1$ [45]. These phase shifts are then transformed into phase shifts defined by Ponomarev and Somov [46] Δ_{pm} and used to obtain continuum states with incoming boundary condition [47]

$$\Phi_{\mathbf{k}}^{(-)} = \frac{1}{k}\sum_{m=-\infty}^{\infty}\sum_{p=|m|}^{\infty} i^p e^{-i\Delta_{pm}} \times \mathcal{Y}_{pm}(\eta,\varphi)\mathcal{Y}_{pm}^*(\theta_k,\varphi_k)\Pi_{|m|q}(\xi,k), \quad (31)$$

where $\mathcal{Y}_{pm}(\eta,\varphi) = \Xi_{|m|q}(\eta)\frac{e^{im\varphi}}{\sqrt{2\pi}}$ are "spheroidal harmonics", Δ_{pm} are the two-center Coulomb phase shifts, and $p = |m| + q$. Continuum states defined by (31) are normalized in the momentum space according to the relation $\langle\Phi_{\mathbf{k}}^{(-)}|\Phi_{\mathbf{k}'}^{(-)}\rangle = \delta(\mathbf{k}-\mathbf{k}')$.

The photoelectron angular distribution (PAD) is obtained as

$$\frac{d^3P}{d\Omega_k dE} = k|\langle\Phi_{\mathbf{k}}^{(-)}|\Psi(t_f)\rangle|^2. \quad (32)$$

The integration over ξ coordinate in the PAD (32) is carried out with Gauss-Legendre quadrature points. We have found that the number of terms in the summation over p in (31) must at least be equal to the number of spherical harmonics used in the TDSE solver in order to obtain converged PAD. Alternatively, the photoelectron spectrum can be obtained by the window-operator technique [48,49], which is a very convenient way to calculate photoelectron spectra without explicit computation of the unperturbed Hamiltonian's continuum eigenfunctions. We have also used this method to calculate ATI spectra (see [50]). In the present paper all the ATI spectra are obtained by the projection method at the equilibrium internuclear distance $R = 2$ a.u.

In Fig. 4 we present the ATI spectra along the laser polarization direction, obtained for the wavelength $\lambda = 400$ nm ($\omega = 0.1138$ a.u.) and laser field intensity $I = 3.5 \times 10^{14}$ W/cm^2, using $1\sigma_g$ as the initial state. The spectra are obtained using a trapezoidal electric field $E(t) = -E_0 f(t)\sin(\omega t)$, where pulse

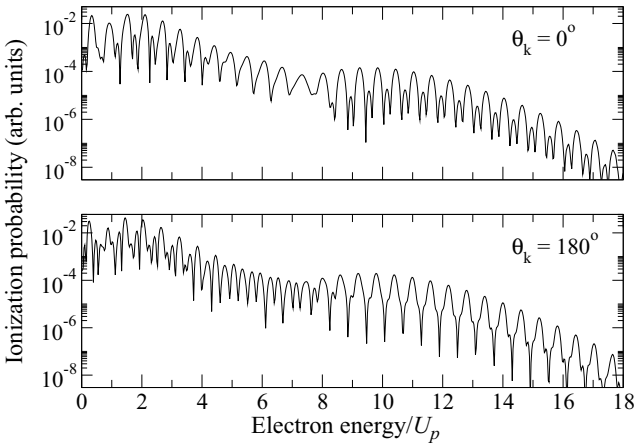

FIG. 4. Ionization probability along the laser polarization direction for the initial state $1\sigma_g$, obtained with the trapezoidal laser pulse envelope. Laser parameters are $I = 3.5 \times 10^{14}$ W/cm^2, $\lambda = 400$ nm ($\omega = 0.1138$ a.u.).

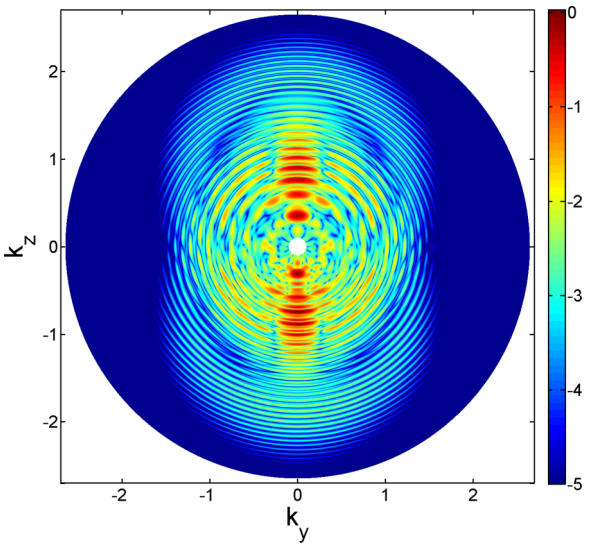

FIG. 5. The logarithm of the photoelectron angular distribution for the same laser field parameters as in Fig. 4. The false color scale covers five orders of magnitude.

envelope $f(t)$ is given by

$$f(t) = \begin{cases} \frac{t}{n_r T}, & 0 \leqslant t \leqslant n_r T, \\ 1, & n_r T \leqslant t \leqslant (n_r + n_c)T, \\ \frac{(2n_r+n_c)T-t}{n_r T}, & (n_r + n_c)T \leqslant t \leqslant (2n_r + n_c)T, \end{cases} \tag{33}$$

where $T = 2\pi/\omega$. We have used $n_r = 0.5$ and $n_c = 4$.

Due to very high ionization potential of the ground state $1\sigma_g$ ($I_p = 30$ eV) at the equilibrium internuclear distance, the intensity of the laser field has to be very high in order to have a substantial ionization probability. On the other hand, higher intensity means more basis functions and a larger grid has to be used in order to obtain a converged time-dependent wave function.

At this wavelength and intensity we expect to see a spectrum corresponding to high-order above-threshold ionization (HATI) [51,52]. In Fig. 4, four distinct regions are clearly visible in the spectra. The region up to approximately $3U_p$ is the ATI spectrum which corresponds to the direct electrons (ionization probability is of the order 10^{-2} arb. units). This is followed by a transition region from the direct to the rescattered electrons. Next, the plateau region, with the ionization probability approximately two orders of magnitude lower than that of the direct electron, extends from $4U_p$ up to approximately $10U_p$ and represents the rescattered electrons. Finally, after the cutoff, which is at the energy $10.007U_p + 0.538I_p$ according to the semiclassical formula from [53], the ionization probability exponentially decreases.

In Fig. 5 we show the PAD corresponding to the above parameters. As we can notice, the presented PAD clearly manifests typical ATI rings separated by photon energy. The cutoff for $k_y = 0$ and $k_z = \sqrt{20U_p} = 1.96$ a.u. is clearly visible. The spectra are calculated using 55 spherical harmonics, with grid extending to $\xi_{\max} = 600$, and for $N_\xi = 1209$, leading up to about 55 000 basis functions in (10).

As the last example we show HATI spectra obtained for the $1\sigma_u$ initial state and $I = 10^{14}$ W/cm^2, $\lambda = 800$ nm ($\omega = 0.0569$ a.u.) (Figs. 6 and 7). Since the wavelength is longer than in the previous calculations, the plateau region is more pronounced. The spectra are calculated using 35 spherical harmonics, with grid extending to $\xi_{\max} = 1000$, and for $N_\xi = 1009$.

VI. SUMMARY

In the present paper we have described a numerical method for solving the TDSE for molecular hydrogen cation in a linearly polarized laser field. It is assumed that the laser field is polarized along the molecular axis. The method is based on the expansion of the time-dependent wave function in a basis of B-spline functions and spherical harmonics in prolate spheroidal coordinates. The time evolution of the initial state is performed by a Crank-Nicolson propagator.

In order to test the accuracy of our numerical method we have calculated the energies of the several lowest lying bound states. We have also calculated HHG spectra for different

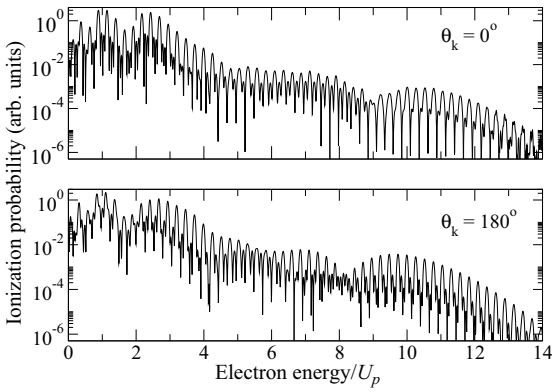

FIG. 6. Ionization probability along the laser polarization direction for initial state $1\sigma_u$, obtained with trapezoidal laser pulse envelope. Laser parameters are $I = 10^{14}$ W/cm^2, $\lambda = 800$ nm ($\omega = 0.0569$ a.u.).

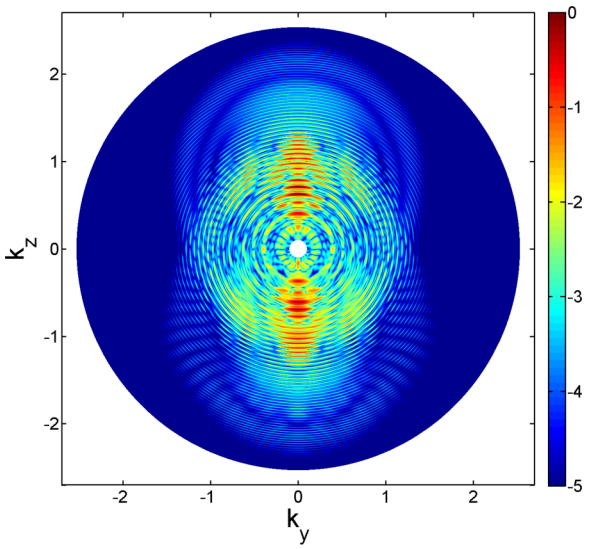

FIG. 7. The logarithm of the photoelectron angular distribution for the same laser field parameters as in Fig. 6.

laser field intensities using different initial bound states. The produced HHG spectra are gauge invariant and the position of the cutoff is in agreement with the semiclassical prediction.

As the final test, we reported calculations of the photoelectron ionization probability. Ionization probability is calculated by projecting the final wave function onto the continuum states with an incoming boundary condition. In the spectra we observed clearly resolved ATI peaks (Fig. 4) with four clearly visible distinct regions. The region up to $3U_p$ corresponds to the direct ATI electrons. This region is followed by a transition region from the direct to the rescattered electrons. The plateau region extends from $4U_p$ up to approximately $10U_p$ and represents rescattered electrons. Finally, the cutoff region corresponds to the energies larger than $10.007U_p + 0.538I_p$. We are not aware of any publication in which the high-energy electron spectra with a plateau and clear cutoff were obtained from the solution of the three-dimensional TDSE for molecules.

Insights into symmetry related effects involving the highest-occupied molecular orbitals of complex molecules can be gained by studying their symmetry analog for H_2^+, and this fact increases the importance of the method developed in our paper.

ACKNOWLEDGMENTS

We thank Prof. Dr. Dieter Bauer and Julius Rapp for providing access to a high-performance computing workstation at the Institute of Physics, University of Rostock.

[1] M. Lein, Molecular imaging using recolliding electrons, J. Phys. B: At. Mol. Opt. Phys. **40**, R135 (2007).
[2] P. Agostini and L. F. DiMauro, Atomic and molecular monization dynamics in strong laser fields: From optical to x-rays, Adv. At. Mol. Opt. Phys. **61**, 117 (2012).
[3] M. Kohler, T. Pfeifer, K. Hatsagortsyan, and C. Keitel, Frontiers of atomic high-harmonic generation, Adv. At. Mol. Opt. Phys. **61**, 159 (2012).
[4] K. C. Kulander, K. J. Schafer, and J. K. Krause, in *Atoms in Intense Laser Fields*, edited by M. Gavrila (Academic, New York, 1992), pp. 247–300.
[5] K. C. Kulander, K. J. Schafer, and J. L. Krause, in *Super-Intense Laser-Atom Physics*, edited by B. Piraux, A. L'Huillier, and K. Rzążewski, NATO Advanced Science Institutes Series, Series B: Physics, Vol. 316, (Plenum, New York 1993), pp. 95–110.
[6] M. Protopapas, C. H. Keitel, and P. L. Knight, Atomic physics with super-high intensity lasers, Rep. Prog. Phys. **60**, 389 (1997).
[7] D. Bauer and P. Koval, Qprop: A Schrödinger-solver for intense laser–atom interaction, Comput. Phys. Commun. **174**, 396 (2006).
[8] S. Patchkovskii and H. G. Muller, Simple, accurate, and efficient implementation of 1-electron atomic time-dependent Schrödinger equation in spherical coordinates, Comput. Phys. Commun. **199**, 153 (2016).
[9] X. M. Tong, Z. X. Zhao, and C. D. Lin, Theory of molecular tunneling ionization, Phys. Rev. A **66**, 033402 (2002).
[10] J. Muth-Böhm, A. Becker, and F. H. M. Faisal, Suppressed Molecular Ionization for a Class of Diatomics in Intense Femtosecond Laser Fields, Phys. Rev. Lett. **85**, 2280 (2000).
[11] D. B. Milošević, Strong-field approximation for ionization of a diatomic molecule by a strong laser field, Phys. Rev. A **74**, 063404 (2006).
[12] S. Odžak and D. B. Milošević, Interference effects in high-order harmonic generation by homonuclear diatomic molecules, Phys. Rev. A **79**, 023414 (2009).
[13] M. Busuladžić, A. Gazibegović-Busuladžić, D. B. Milošević, and W. Becker, Angle-Resolved High-Order Above-Threshold Ionization of a Molecule: Sensitive Tool for Molecular Characterization, Phys. Rev. Lett. **100**, 203003 (2008).
[14] E. Hasović and D. B. Milošević, Strong-field approximation for above-threshold ionization of polyatomic molecules. II. The role of electron rescattering off the molecular centers, Phys. Rev. A **89**, 053401 (2014).
[15] Y. V. Vanne and A. Saenz, Numerical treatment of diatomic two-electron molecules using a B-spline based CI method, J. Phys. B: At. Mol. Opt. Phys. **37**, 4101 (2004).
[16] G. L. Kamta and A. D. Bandrauk, Three-dimensional time-profile analysis of high-order harmonic generation in molecules: Nuclear interferences in H_2^+, Phys. Rev. A **71**, 053407 (2005).
[17] D. A. Telnov and S. I. Chu, *Ab initio* study of the orientation effects in multiphoton ionization and high-order harmonic generation from the ground and excited electronic states of H_2^+, Phys. Rev. A **76**, 043412 (2007).
[18] J. Fernández and L. B. Madsen, Alignment dependence in above-threshold ionization of H_2^+: Role of intermediate resonances, J. Phys. B: At. Mol. Opt. Phys. **42**, 085602 (2009).
[19] M. Murakami and S.-I. Chu, Photoelectron momentum distributions of the hydrogen molecular ion driven by multicycle near-infrared laser pulses, Phys. Rev. A **94**, 043425 (2016).

[20] M. Aubert, N. Bessis, and G. Bessis, Prolate-spheroidal orbitals for homonuclear and heteronuclear diatomic molecules. I. Basic procedure, Phys. Rev. A **10**, 51 (1974).
[21] E. A. McCullough, Jr., Numerical Hartree-Fock methods for diatomic molecules: A partial-wave expansion approach, Comput. Phys. Rep. **4**, 265 (1986).
[22] L. Laaksonen, P. Pykkö, and D. Sundholm, Fully numerical Hartree-Fock methods for molecules, Comput. Phys. Rep. **4**, 313 (1996).
[23] I. N. Levine, *Quantum Chemistry*, 5th ed. (Prentice Hall, Englewood Cliffs, NJ, 2000).
[24] H. Bachau, E. Cormier, P. Decleva, J. E. Hansen, and F. Martín, Applications of B-splines in atomic and molecular physics, Rep. Prog. Phys. **64**, 1815 (2001).
[25] L. Tao, C. W. McCurdy, and T. N. Rescigno, Grid-based methods for diatomic quantum scattering problems: A finite-element discrete-variable representation in prolate spheroidal coordinates, Phys. Rev. A **79**, 012719 (2009).
[26] B. Zhang, J. Yuan, and Z. X. Zhao, Alignment-dependent ionization of H_2^+: From multiphoton ionization to tunneling ionization, Phys. Rev. A **85**, 033421 (2012).
[27] I. S. Gradshteyn and I. M. Ryzhik, *Table of Integrals, Series and Products*, 5th ed. (Academic, New York, 1994).
[28] W. H. Press, S. A. Teukolsky, W. T. Vetterling, and B. P. Flannery, *Numerical Recipes in Fortran 77: The Art of Scientific Computing*, 2nd ed. (Cambridge University Press, New York, 1992).
[29] E. Anderson *et al.*, *LAPACK User's Guide*, 3rd ed. (SIAM, Philadelphia, 1999).
[30] D. M. Telnov and S.-I. Chu, Time-dependent generalized pseudospectral method for accurate treatment of multiphoton processes of diatomic molecules in intense laser fields, Comput. Phys. Commun. **182**, 18 (2011).
[31] H. Muller, An efficient propagation scheme for the time-dependent Schrödinger equation in the velocity gauge, Laser Phys. **9**, 138 (1999).
[32] L. Tao, C. W. McCurdy, and T. N. Rescigno, Grid-based methods for diatomic quantum scattering problems. II. A finite-element discrete-variable representation in prolate spheroidal coordinates, Phys. Rev. A **80**, 013402 (2009).
[33] D. Neuhasuer and M. Baer, The time-dependent Schrödinger equation: Application of absorbing boundary conditions, J. Chem. Phys. **90**, 4351 (1989).
[34] http://www.openblas.net/.
[35] https://software.intel.com/en-us/intel-mkl.
[36] P. B. Corkum, Plasma Perspective on Strong Field Multiphoton Ionization, Phys. Rev. Lett. **71**, 1994 (1993).
[37] M. Lewenstein, P. Balcou, M. Y. Ivanov, A. L'Huillier, and P. B. Corkum, Theory of high-harmonic generation by low-frequency laser fields, Phys. Rev. A **49**, 2117 (1994).
[38] D. B. Milošević, Cut-off law for high-harmonic generation by an elliptically polarized laser field, J. Phys. B: At. Mol. Opt. Phys. **33**, 2479 (2000).
[39] A. D. Bandrauk, S. Chelkowski, D. J. Diestler, J. Manz, and K.-J. Yuan, Quantum simulation of high-order harmonic spectra of the hydrogen atom, Phys. Rev. A **79**, 023403 (2009).
[40] E. Cormier and P. Lambropoulos, Optimal gauge and gauge invariance in non-perturbative time-dependent calculation of above-threshold ionization, J. Phys. B: At. Mol. Opt. Phys. **29**, 1667 (1996).
[41] P. Agostini, F. Fabre, G. Mainfray, G. Petite, and N. K. Rahman, Free-Free Transitions Following Six-Photon Ionization of Xenon Atoms, Phys. Rev. Lett. **42**, 1127 (1979).
[42] D. Yan, L.-Y. Peng, and Q. Gong, Grid method for computation of generalized spheroidal wave functions based on discrete variable representation, Phys. Rev. E **79**, 036710 (2009).
[43] J. P. Killingbeck, *Microcomputer Quantum Mechanics*, (Adam Hilger, Bristol, 1983).
[44] G. Hadinger, M. Aubert-Frécon, and G. Hadinger, Continuum wavefunctions for one-electron two-centre molecular ions from the Killingbeck-Miller method, J. Phys. B: At. Mol. Opt. Phys. **29**, 2951 (1996).
[45] J. Rankin and W. R. Thorson, Continuum wave functions for the two-center, one-electron system, J. Comput. Phys. **32**, 437 (1979).
[46] L. I. Ponomarev and L. N. Somov, The wave functions of continuum for the two-center problem in quantum mechanics, J. Comput. Phys. **20**, 183 (1976).
[47] X. Guan, K. Bartschat, and B. I. Schneider, Breakup of the aligned H_2 molecule by xuv laser pulses: A time-dependent treatment in prolate spheroidal coordinates, Phys. Rev. A **83**, 043403 (2011).
[48] K. J. Schafer and K. C. Kulander, Energy analysis of time-dependent wave functions: Application to above-threshold ionization, Phys. Rev. A **42**, 5794 (1990).
[49] K. J. Schafer, The energy analysis of time-dependent numerical wave functions, Comput. Phys. Commun. **63**, 427 (1991).
[50] B. Fetić and D. B. Milošević, Numerical solution of the time-dependent Schrödinger equation for molecular hydrogen ion in linearly polarized laser field, AIP Conf. Proc. **1722**, 200006 (2016).
[51] G. G. Paulus, W. Nicklich, H. Xu, P. Lambropoulos, and H. Walther, Plateau in Above Threshold Ionization Spectra, Phys. Rev. Lett. **72**, 2851 (1994).
[52] D. B. Milošević, G. G. Paulus, D. Bauer, and W. Becker, Above-threshold ionization by few-cycle pulses, J. Phys. B: At. Mol. Opt. Phys. **39**, R203 (2006).
[53] M. Busuladžić, A. Gazibegović-Busuladžić, and D. B. Milošević, High-order above-threshold ionization in a laser field: Influence of the ionization potential on the high-energy cutoff, Laser Phys. **16**, 289 (2006).